Geologie en Mijnbouw 64: 271-280 (1985).

Directional variations of fold axes in progressive deformation, an example from a Betic fold nappe in S Spain

Ruud Weijermars
Department of Mineralogy and Petrology, Institute of Geology, University of Uppsala, Box 555, S-75122 Uppsala, Sweden

Manuscript received 1 February 1985; accepted in revised form 8 August 1985

Abstract

Weijermars, R. 1985 Directional variations of fold axes in progressive deformation, an example from a Betic fold nappe in S Spain – Geol. Mijnbouw 64: 271-280.

Singly folded and *coaxially* refolded rocks generally have axial directions that plot as unimodal clusters and either small or great circle girdles. Cluster distributions of axes are characteristic of either cylindrical folds or sheath folds developed at high shear strains. Girdle distributions may occur due to conical folding or sheath folds developed at intermediate shear strains. A variety of axial distributions can occur in *non-coaxially* refolded regions, since the variation of the axes of folds due to refolding depends on the initial interlimb angle and the angle between the older and younger axial planes. Characteristic fold axial distributions are summarised in a practical chart for general application (Table 1).

This study is illustrated by the analysis of axial directions of isoclinal minor folds cogenetic with the final emplacement of the Aguilón fold nappe in S Spain. The axial directions of these (D_s) folds show a bimodal girdle distribution which is ascribed to their superposition on opposing limbs of the preceding (D_r) folds. Directional statistics suggests that D_r folds were of chevron or similar type with interlimb angles of about 65 degrees before they all but disappeared after non-coaxial isoclinal D_s refolding.

Introduction

The orientations of fold axes and any axial intersection lineation are commonly used to investigate the geometry of folds. In *singly folded* rocks two characteristic distributions of fold axes on a stereogram may occur: 1) strong unimodal clusters of cylindrical folds and 2) small-circle distributions of conical folds due to their non-parallel fold axes (cf. Ramsay 1967). The closer the conical folds approach a cylindrical form, the smaller the girdle becomes.

Folds with variable fold axial orientations have been investigated by Cobbold & Quinquis (1980). According to these authors, fold shapes in systems where the bulk deformation is a progressive *homogeneous* simple shear, may become strongly non-cylindrical or sheath-like at high shear strains. Small local perturbations in an initially planar layering may be amplified by high shear to sheath folds even in regimes where the bulk homogeneous shear is parallel to overall bedding (cf. Platt 1983), see Figure 1a. Characteristically the axes of such folds are curved within the axial planes at high shear strain and statistical analysis of their axial directions shows a strong maximum centered about

the maximum principal extension axis of the bulk strain ellipsoid (Bell 1978; Cobbold & Quinquis 1980).

Statistical analysis of axial directions of mature sheath folds may therefore yield unimodal clustering of the axes and falsely suggest a cylindrical fold geometry. At lower shear strains, sheath fold axes can be expected to vary in orientation from a good point cluster about the Y direction (parallel to the intermediate axis of the shear strain ellipsoid, when the fold just starts to depart from the cylindrical stage) through a great circle girdle distribution at intermediate strains, to a point cluster in the X direction at high shear strains. Significantly the axes plot along great-circles and not along small-circles as in the conical fold types, since the former axes lie within a single plane and the latter do not.

Yet another type of non-cylindrical fold may occur as a result of folding with a component of *inhomogeneous* shortening strain as indicated in Figure 1b. This is a very special type of inhomogeneous strain since horizontal simple shear gradients occur within vertical axial surfaces. Such a fold model has been suggested to account for axial variations observed in the Padstow structure in Cornwall (Gauss 1973). As is the case in sheath folds, Gauss' model predicts that the axial directions would approach the axis of greatest extension with increasing strain. Great-circle distributions may occur in this particular fold type also.

The determination of fold geometry from the distribution of fold axes (and any parallel intersection lineations) is much more complex in *refolded* rocks. In all ordinary cases of single progressive strain the axes lie in clusters or in small-circle girdles (partial or complete). Great-circle girdles may occur if fold types indicated in Figure 1 occur. This is more complicated in non-coaxially refolded rocks. The new folds generated on already folded surfaces will have patterns of axial directions which depend on the tightness, style and relative attitude of the older folds. Noteworthy, the new axes are invariably great-circle populations if the refolding

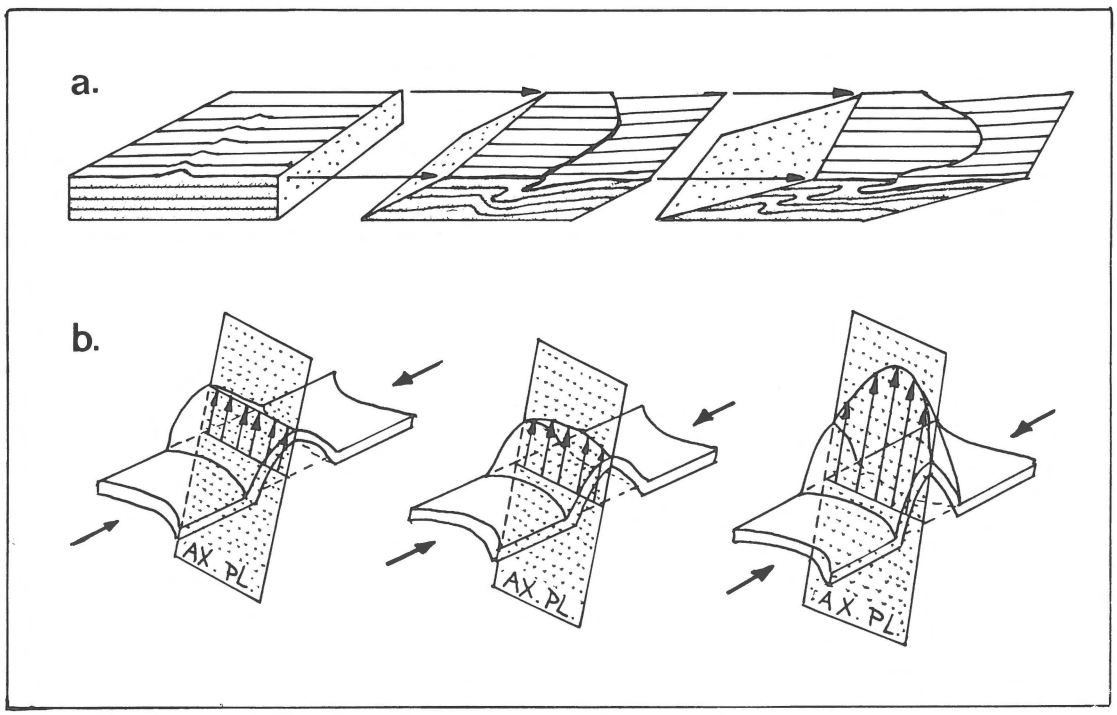

Fig. 1. Modes in which dome folds may develop.
a) Homogeneous simple shear strain superimposed on a planar fabric with initial non-cylindrical deflections from planarity (after Cobbold & Quinquis 1980, fig. 2).
b) Inhomogeneous compressive strain. No initial planar imperfections are needed (after Gauss 1973, fig. 17).

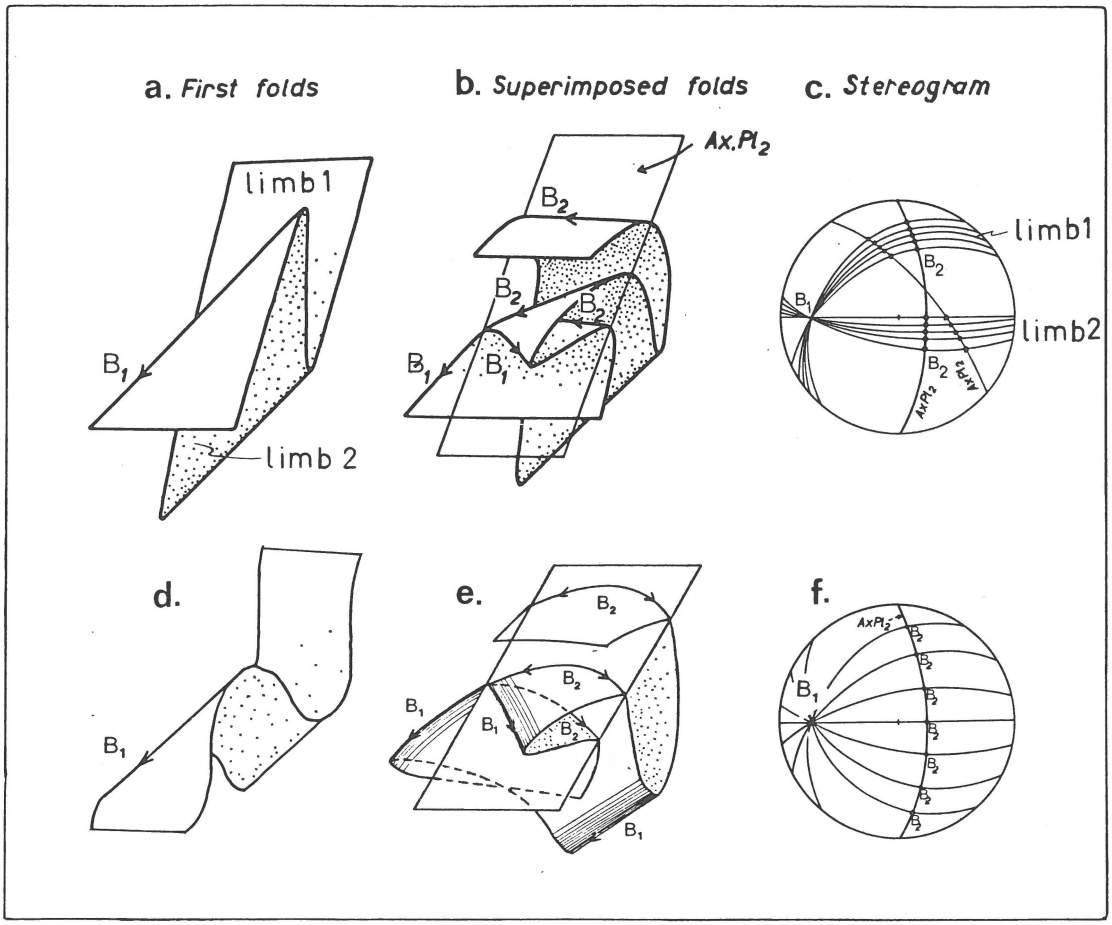

Fig. 2. a) First generation folds of chevron type.
b) Non-coaxial cylindrical refolding of the folds in (a) will result in second generation fold axes (B_2) with two different directions. The angle between the two sets of B_2 axes depends upon the angle between the axial planes and fold axes of the first and second folds. The angle between B_2 axes is visible within axial planes of second generation folds (Ax Pl 2), even where F_1-fold closures would be tightening in the course of refolding by axial planar shear.
c) The folded surface in (a) plots as two great-circle girdles on a stereogram. The orientation of B_2-fold axes depends upon the manner in which Ax Pl 2 cuts the limbs of first generation folds. Two examples of possible Ax P1 2 orientations are shown. Two strong B_2-clusters appear if the first folds are of chevron type.
d) First generation concentric folds.
e) Non-coaxial cylindrical refolding of the concentric folds in (d) give two sets of curved fold axes B_2.
f) Concentric fold surface in (d) plots on a stereogram as planes with a wide range of orientations. The fold axes B_2 will have orientations depending upon the manner in which Ax Pl 2 cuts the undisturbed first generation folds (partly after Ramsay 1967, figs. 10.22 and 10.23).

is cylindrical because all newly formed axes lie within the younger axial plane (Fig. 2).

Axial distributions and their respective fold geometries which may occur within rocks folded once or twice are summarised in Table 1. The term *coaxial* is used here to indicate that new axes of cylindrical folds have the same orientation but are not coincident with older fold axes; it does not refer to the principal axes of strain ellipsoids. Conical folds are termed coaxial with older folds if the axes within the axial planes of conical folds are parallel with those of older folds. The two fold types depicted in Figure 1 are termed dome folds. Refolding by dome folds could start as coaxial but can never remain so; the old and new fold axes (B_1 and B_2, respectively) always become non-coaxial

after any finite deformation. Although being non-coaxial, B_1 and B_2 may lie in planes which remain parallel during progressive deformation. A distinction has therefore been made between *coplanar* and *non-coplanar* refolding by dome folds. Non-coplanar refolding implies that the axial planes of the dome folds (Ax Pl 2) are oblique to B_1. Coplanar refolding implies that all B_1 axes are parallel with Ax Pl 2.

The original geometry of older folds can be deduced by analysis of the axial directions of non-coaxially superposed younger folds (Table 1). The method used for obtaining such information from the variation in axial orientation of the new folds was first suggested by Ramsay (1967, p. 539-540). However, it may be difficult to distinguish between great-circle distributions due to non-coaxial cylindrical refolding (Fig. 2) and those due to refolding by dome folds. The problem is illustrated by a practical example from the Sierra Alhamilla in Spain.

Structural background

Several overthrust units are recognised within the Internal or Betic Zone of the Alpine fold belt in southern Spain. The Aguilón nappe represents a higher Betic Unit. It is exposed in the Sierra Alhamilla (Fig. 3a) as a disrupted north-closing fold nappe which overlies lower Betic Units. The

Table 1. Possible axial distributions and corresponding fold geometries in singly folded and in refolded rocks. The term dome folds includes sheath folds and the Gauss' folds illustrated in Figure 1.

Types of distribution of youngest axial directions	Possible fold types indicated by the particular distributions			
	In singly folded rocks	In refolded rocks		
		Superposed folds (D_2)		*Primary fold (D_1) geometry*
		Orientation	*Type*	*assuming cylindrical folding*
A. Unimodel cluster	– cylindrical folds	– coaxial	cylindric	any
		– non-coaxial	cylindric	isoclinal
	– dome folds at high strain	– any	dome folds at high strain	any
B. Small circle girdle	– conical folds	– coaxial	conical	any
		– non-coaxial	conical	isoclinal
C. Full great circle girdle	– dome folds at low strain	– non-coaxial	cylindric	concentric
		– coplanar	dome folds at low strain	any
		– any	dome folds at low strain	isoclinal
D. Great circle girdle with two maxima	– dome folds at intermediate strain	– non-coaxial	cylindric	chevron/similar
		– coplanar	dome folds at intermediate strain	any
		– any	dome folds at intermediate strain	isoclinal
E. Great circle girdle with four maxima	– –	– non-coplanar	dome folds at low and intermediate strain	chevron/similar
F. Random	–	– non-coaxial	conic	any but isoclinal
		– non-coplanar	dome folds at low and intermediate strain	concentric

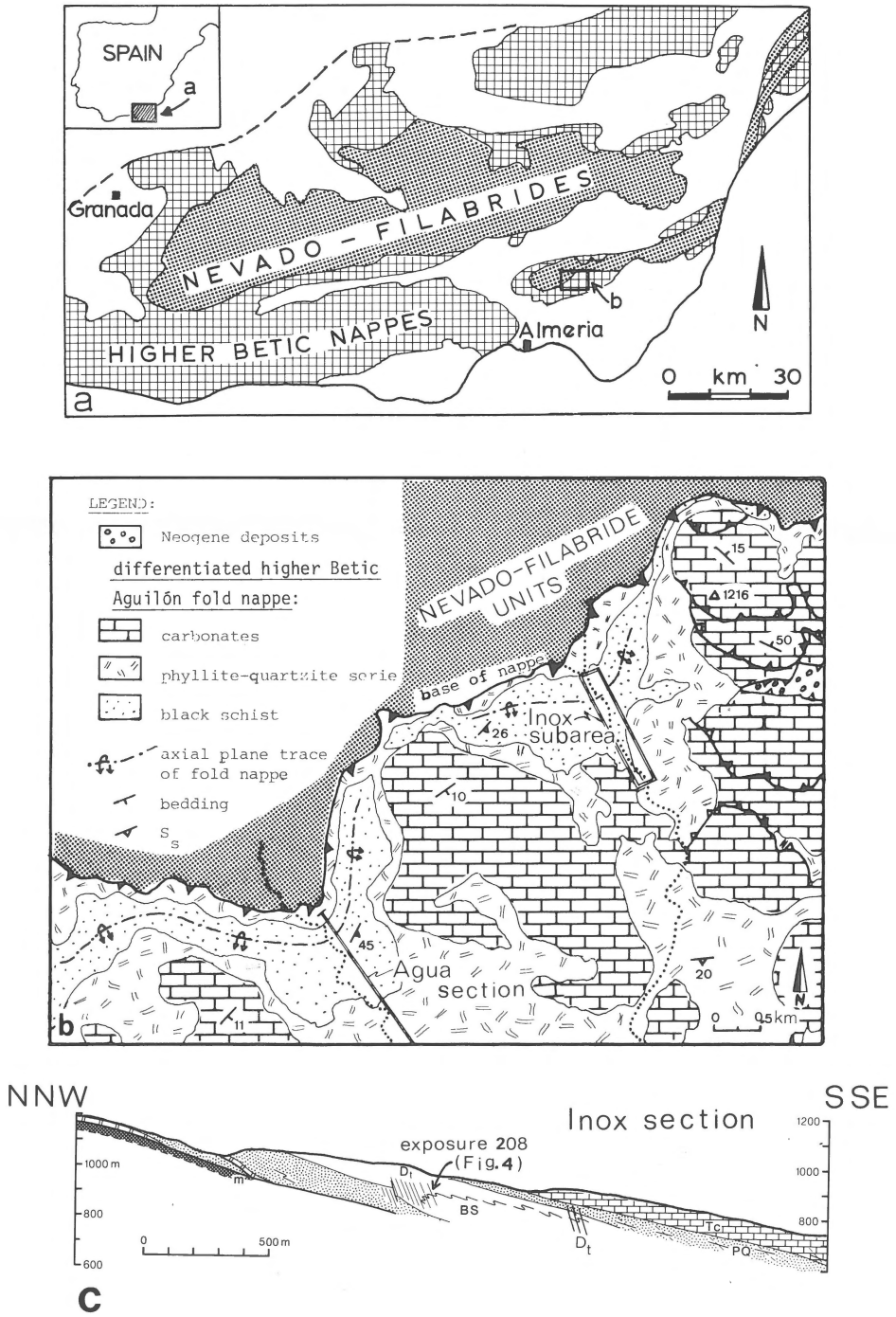

Fig. 3. a) Tectonic sketch map of the eastern Betic Zone, the metamorphic segment of the Betic orogen.
b) Simplified geological map of the central part of the Sierra Alhamilla indicated in (a), showing the locations mentioned in the text.
c) Cross section along the Rambla del Inox through the Aguilón fold nappe as exposed in the Inox subarea showing the Nevado-Filabride Unit (m) at the base of the fold nappe. The fold nappe has a core of black mica schist (BS) and the upper and lower limbs comprise a phyllite-quartzite serie (PQ) and Triassic carbonates (Tc).

general structural history of this nappe is discussed elsewhere (Platt et al. 1983).

A structural section has been analysed in the Rambla del Inox about 3 km northeast of the section in the Rambla del Agua (Fig. 3b) that was studied by Platt (1982). The Inox section cuts the core of the Aguilón nappe (Fig. 3c) which consists of alternating low-grade phyllites and quartzites folded around medium-grade black mica schists.

Three prominent deformation phases have been distinguished in these rocks. Sets of structural elements which are genetically identical have been characterized by an arbitrary letter subscript: D_r (pre-nappe), D_s (main-nappe-forming event) and D_t (a minor and localised post-nappe folding). The structural sets have not been numbered since it is not known whether or not the oldest recognised cleavage fabric S_r is due to overprinting of an older tectonic fabric. In the Inox section only three (metre-scale) D_r minor folds have been recognised, all occurring in one exposure. These folds are isoclinal with axial trends of about 020/30, and are thoroughly overprinted by S_s.

Three penetrative cleavage fabrics, S_r, S_s and S_t, are distinguished. Of these, S_r and S_s have been observed in all outcrops and in samples from the Inox area, whereas S_t is only locally prominent. Both S_r and S_s are crenulation cleavages and either may be the more prominent at particular localities. D_t folds have no axial-plane fabric in the black schist of medium metamorphic grade, but in the overlying phyllite and quartzite sequence D_t structures include a locally well-defined spaced cleavage S_t.

The individual sets of structures correlate well with those described by Platt (1982) in the Agua section, though D_s folds (Platt's 'main-phase' folds) are tighter in the Inox area and become isoclinal (Fig. 4). The orientation of D_s fold axes (B_s) varies over a wide range on the mesoscopic exposure scale (about 20 m^2, cf. Fig. 4). The azimuth of B_s in the phyllite-quartzite sequence may vary as much as 88 degrees, whereas a maximum difference of 68 degrees has been observed in the black mica schist. On the megascopic scale of the entire Inox section, the variability in azimuth is somewhat larger (Fig. 5b). Platt (1982) reported from his section in the Rambla del Agua a significant difference in trend of D_s fold axes between the black mica schists of medium metamorphic grade and the overlying lower-grade phyllite and quartzite sequences. However, no such spatial relationship was recognised in the Inox section.

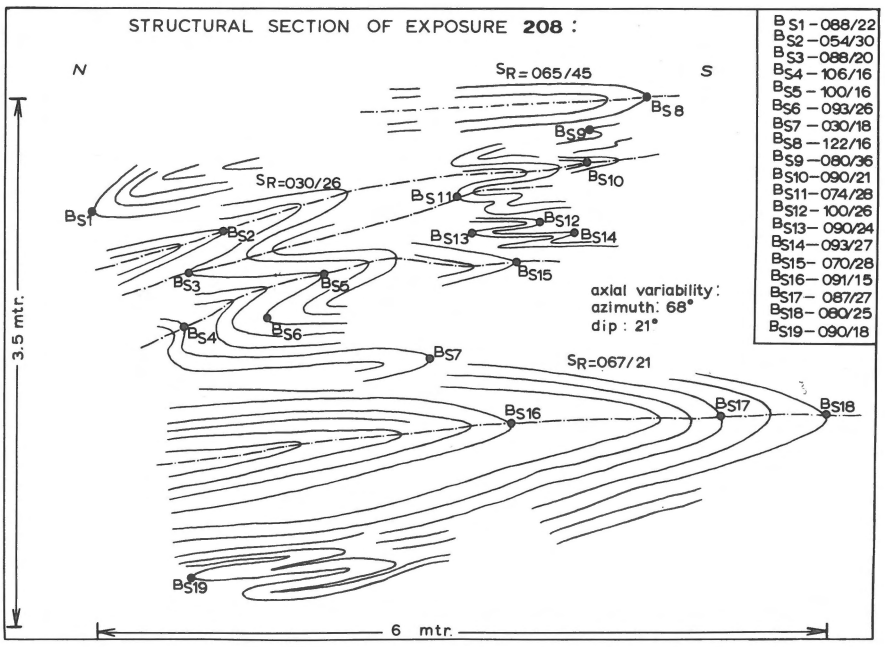

Fig. 4. Field sketch of D_s folds, illustrating their tight-to-isoclinal geometry. Scales are near the outline.

Testing procedure

In areas adjacent to the section analysed here it has been observed that post-D_s structures (e.g. D_t) are only local and of little significance (cf. Platt et al. 1983; Platt 1982). To justify the interpretation of a clear-cut relationship between the range in orientations of B_s (the axes of D_s folds) and the original geometry of the earlier D_r folds it is necessary to confirm that they have not been reoriented by the younger D_t structures in the Inox section (cf. Fig. 3c). The problem is treated statistically in order to simplify the variable directions of the particular structural elements.

Statistical testing was carried out according to the statistical theories of Watson & Fisher (see Mardia 1972). Techniques to obtain the eigen values and eigen vectors of spherical distributions can be found in books on multivariate analysis and the computer programs for this purpose are commonly provided in packages. The properties of eigen values e_1, e_2 and e_3 of Watson's matrix are $e_1+e_2+e_3 = 1$ and $e_1 \leqq e_2 \leqq e_3$. Either the direction of the eigen vector E_1 or E_3, corresponding to the smallest or the largest eigen value, is the best estimate of the mean girdle pole or the mean direction of a cluster (Table 2). When we deal with *clusters* it is possible to calculate mean directions according to Fisher, the maximum likelihood scatter (k) and the reliability cone with half top angle (1-P). The maximum likelihood scatter k can be obtained by the solution of the equation (cf. Mardia 1972)

$$\coth(k) - \frac{1}{k} = \frac{R}{N} \qquad (1)$$

where coth (k) stands for the hyperbolic cotangent of k, R is the sumvector and N is the sample number. The true mean value of population N lies with a probability of (1-P) within a cone of which the axis represents the estimated mean. The half top angle $\alpha_{(1-P)}$ is given by the equation (cf. Mardia 1972)

$$\cos \alpha_{(1-P)} = 1 - \frac{N-R}{R} \left[\left(\frac{1}{P}\right)\frac{1}{N-1} - 1\right] \qquad (2)$$

In the present study (1-P) is taken as 0.95, so that the half top angle α_{95} represents the cone within which lies, with 95 per cent probability, the true mean value.

The relevant statistical constants are calculated for the structural elements of D_s and D_t folds in the Inox section (Table 3). The distributions of S_s, S_t

Table 2. Diagnostic statistic parameters after Mardia (1972, table 8.3).

Nature of the eigen values	Type of distribution	Other features
I. $e_1 \approx e_2 \approx e_3 \approx 0.33$	uniform	axes having no preferred orientation
II. e_3 large e_1, e_2 small	cluster	concentration about eigen vector E_3
– $e_1 \neq e_2$	– asymmetric	"
– $e_1 \approx e_2$	– symmetric	rotational symmetry about E_3
III. e_1 small e_2, e_3 large	girdle	E_1 is pole of the girdle plane
– $e_2 \neq e_3$	– asymmetric	"
– $e_2 \approx e_3$	– symmetric	rotational symmetry about E_1

Table 3. Direction statistics of the Inox area: computer-calculated eigen values, concentration parameter, Watson-mean, Fisher-mean and the reliability area α_{95} (given as the half apical angle).

B_s-L_s N=131	S_s N=104	B_t-L_t N=32	S_t N=24
$e_1 = 0.64$ $e_2 = 0.31$ $e_3 = 0.05$	$e_1 = 0.77$ $e_2 = 0.13$ $e_3 = 0.10$	$e_1 = 0.83$ $e_2 = 0.10$ $e_3 = 0.07$	$e_1 = 0.86$ $e_2 = 0.09$ $e_3 = 0.05$
Watson mean of girdle: 276/65	Watson mean: 284/59	Watson mean: 070/26	Watson mean: 333/44
not applicable because clustering is absent	k = 6.9 Fisher mean: 284/57 $\alpha_{95} = 5.7$	k = 10.0 Fisher mean: 071/27 $\alpha_{95} = 8.5$	k = 10.7 Fisher mean: 330/45 $\alpha_{95} = 9.5$
girdle (bimodal, see Fig. 5b)	cluster	cluster	cluster

and the combined data set of B_t and intersection lineation L_t show good clustering, whereas the eigen values of the combined data set B_s-L_s merely resemble that of a girdle distribution. The sample sizes are large enough to prove the existence of preferred orientations. Woodcock & Naylor (1983, in particular figs. 2, 5 and 9) demonstrated the strength of eigen value tests to establish the significance of preferred orientations, as applied in this paper.

From the density plots of Figure 5a it appears that the fold axes B_t and the intersection lineations L_t lie within the girdle of B_s-L_s (Fig. 5b). The relationship becomes clearer when all the data of Figure 5a are rotated so that the B_t-L_t cluster is in the horizontal plane and the axial planes S_t are vertical (Fig. 5c). The distribution of B_s-L_s (Fig. 5b) is concurrently rotated in a similar manner (Fig. 5d). (The suggested relationship between B_t-L_t and B_s-L_s can be checked by simple stereographic reconstruction using the computed mean values for their cluster and girdle pole, respectively.) The Watson mean of the B_t-L_t cluster (070/26), lies statistically upon the great-circle belonging to the pole of the B_s-L_s girdle which is represented by the eigen vector (276/65) with the largest eigen value. It can thus be safely assumed that the B_s-L_s girdle is *not due to later refolding*.

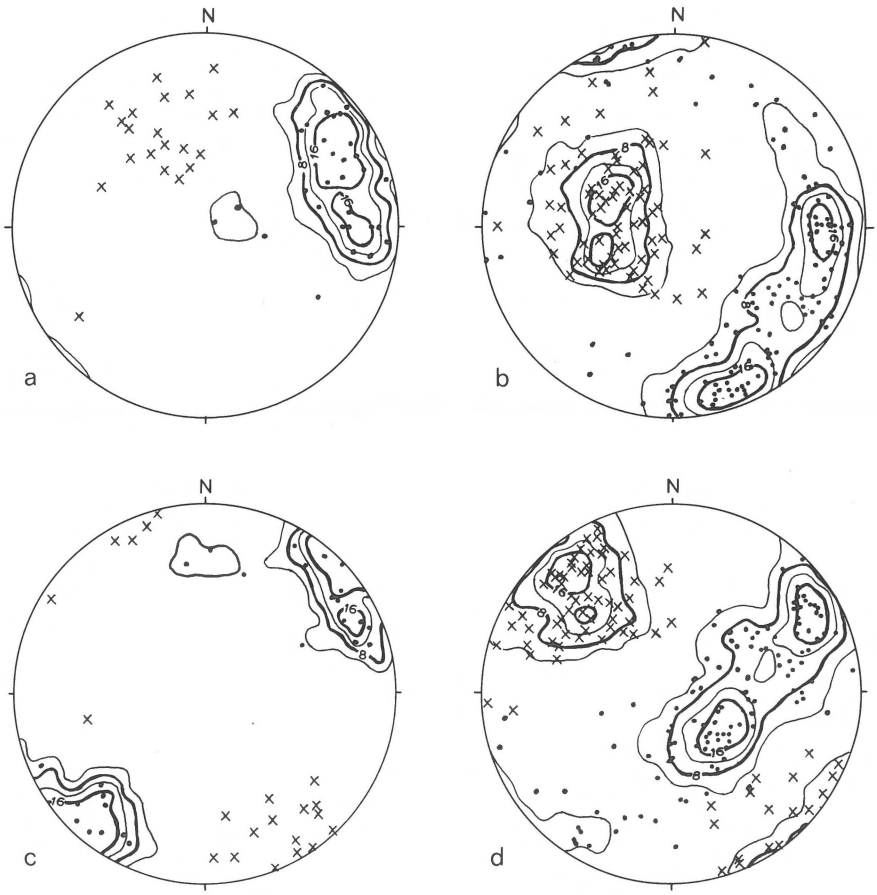

Fig. 5. Density of directional data from the Rambla del Inox contoured by 3-dimensional area counting on the statistical sphere surface. Contouring by 2 per cent of area counting unit, unless otherwise stated.

a) Combined plot of poles to (= π) S_t (crosses, N = 24) and B_t-L_t (dots, N = 26, N = 6). The cluster of πS_t is not contoured because of the small sample set.

b) Combined plot of πS_s (crosses, N = 104) and B_s-L_s (dots, N = 116, N = 15). The bimodal girdle distribution of B_s-L_s is contoured with a 3-per cent of area counting unit for clarity.

c & d) Sample sets of (a) and (b), respectively, after similar rotation so that S_t is vertical and B_t-L_t horizontal.

Discussion and conclusions

The Inox riverbed includes a structural section through the Aguilón nappe, a north-closing recumbent isoclinal fold situated in the Sierra Alhamilla (southeast Spain). The structure of the Aguilón nappe can be determined by vergence changes of congruent minor D_s folds (Platt et al. 1983). These folds are isoclinal and have a well defined axial-plane fabric S_s. Earlier D_r folds are rarely identifiable due to intense flattening by the later D_s folding and overprinting by the cogenetic penetrative S_s fabric.

The geometry of the D_r folds prior to refolding could be determined from the directions of D_s folds axes, but then it is a necessary constraint that D_s folding was originally highly cylindrical. Theoretically, D_s fold axes may plot as a great-circle girdle with maxima due to either non-coaxial cylindrical refolding (Fig. 2) or due to refolding by dome folds (Fig. 1). Non-coplanar refolding by dome folds of first generation chevron or similar type folds could result in a great-circle distribution of the new fold axes, since these lie within their axial planes as well (Fig. 6a-c). However, superposed mature dome folds would give axes that plot either as great-circle

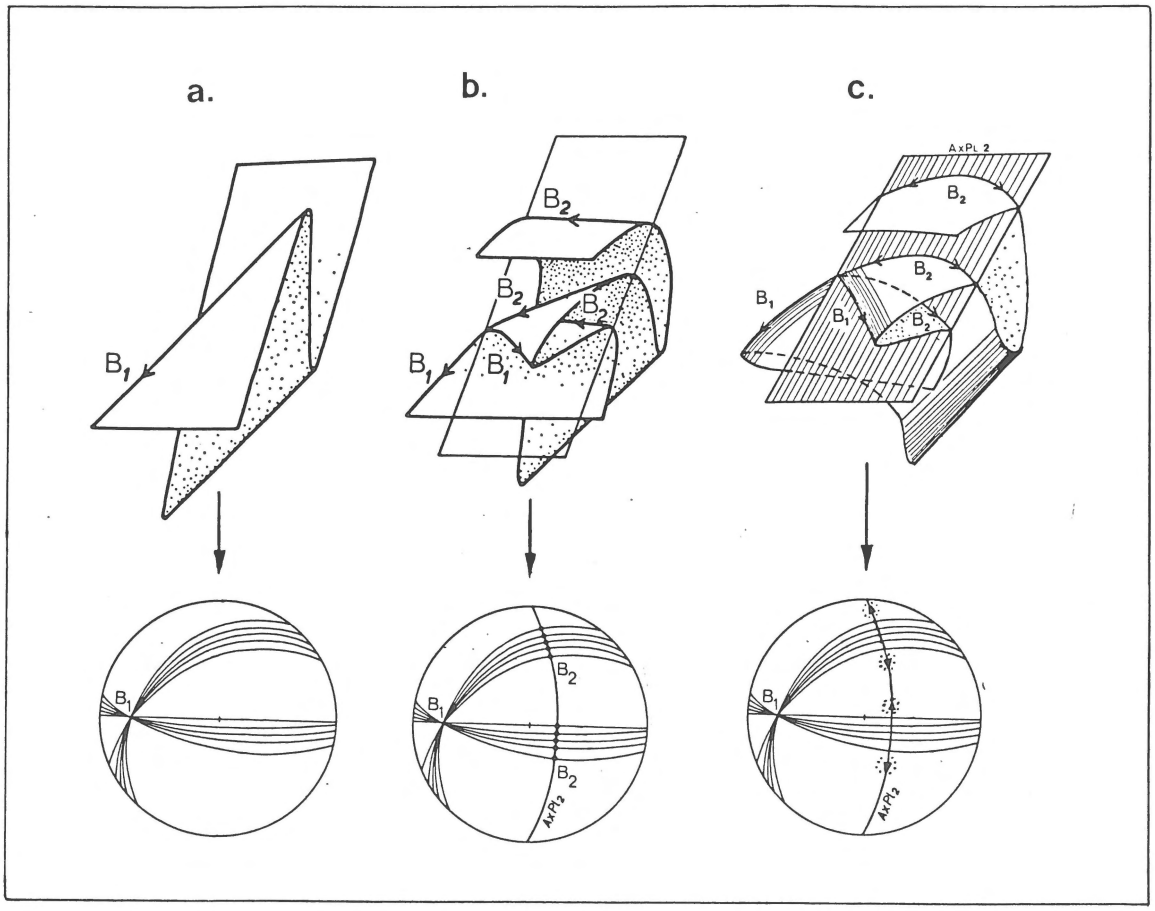

Fig. 6. Successive stages in dome folding of a chevron fold:
a) First generation folds of chevron type could be considered as two sets of parallel planes shown on the stereogram.
b) Refolding by dome folds with an axial plane oblique to B_1 fold axes (non-coplanar). The B_2 fold axes will be straight and look identical to those in Figure 2b at a very early stage of the refolding. The stereogram will then show a bimodal girdle of B_2 fold axes.
c) B_2 fold axes will bend within their axial plane (Ax Pl 2) due to progressive dome folding, still at low strain. The stereogram shows how B_2 fold axes tend to change orientation within Ax Pl 2 during progressive deformation. B_2 fold axes will finally align and plot as a single cluster after high strain by dome folding.

girdles with four maxima or as single points, dependent on the magnitude of the shear strain. Non-coplanar refolding by dome folds at low or intermediate shear strain would give great-circle girdles with four maxima (Table 1, section E).

Table 1 (section D) shows all three possibilities remaining to explain the bimodal great-circle girdle of B_s-L_s observed in the Inox area (Fig. 5b). If the primary folds were isoclinal the superposition effect of dome folds would be identical to the situations illustrated in Figure 1 and the great-circle girdle of the dome fold axes could then yield two maxima at the most. Refolding by dome folds which have axial planes parallel to the fold axes of any type of cylindrical first folds (coplanar refolding) could also yield a bimodal great-circle distribution of dome fold axes after intermediate strain. Nevertheless, the coplanarity is likely to become increasingly unstable during progressive refolding and may be rare in nature. Either of the two types of refolding by dome folds indicated in section D of Table 1 is likely to give a mineral elongation lineation oblique to the dome fold axes similar to that indicated by the vertical lines in the axial plane of Figure 6c. Since such a lineation has not been observed in the Inox area this would appear to preclude the development of sheath type folds or folds due to inhomogeneous shortening.

It seems that the bimodality in D_s fold axial directions (Fig. 5b) can be best explained by non-coaxial superposition of cylindrical folds on older folds having extensive planar limbs and behaving as passive strain markers. The angle of 65 degrees between the maxima in Figure 5b could be used to estimate the maximum angle of the D_r folds prior to refolding (cf. Fig. 2c). If the axial planes of the superposed folds were originally orthogonal to the older fold axes (i.e. orthogonal refolding) then D_r folds may have had interlimb angles of 65 degrees. If the refolding was oblique in this respect then the real interlimb angle may have been less than 65 degrees.

In view of Ramsay's et al. (1983) suggestion that the internal deformation of fold nappes is mostly accomplished by simple shear strains of $\gamma = 4$-10, it is perhaps not surprising that an average D_r interlimb angle which may have been as large as 65 degrees, became isoclinal during the nappe-forming event. Fold nappe development in plane shear strain within a plane parallel to the direction of nappe propagation and with a shear strain $\gamma = 4$ would result in an apparent shortening of 76 per cent, whereas $\gamma = 10$ would give a shortening as large as 99 per cent (using Ramsay 1980, eq. 6).

Acknowledgments

I thank Bernard Bollegraaf of the Amsterdam University, Chris Talbot of the Uppsala University and Martin Jackson of the University of Texas at Austin for suggestions and discussions. Kersti Gløersen typed the final manuscript and the tables in Uppsala.

References

Bell, T.H. 1978 Progressive deformation and reorientation of fold axes in a ductile mylonite zone: the Woodroffe Thrust – Tectonophysics 44: 285-320

Cobbold, P.R. & H. Quinquis 1980 Development of sheath folds in shear regimes – J. Struct. Geol. 2: 119-126

Gauss, G.A. 1973 The structure of the Padstow Area, North Cornwall – Proc. Geol. Ass. 84, part 3: 283-313

Mardia, K.V. 1972 Statistics of directional data – Academic Press (London): 371 pp

Platt, J.P. 1982 Emplacement of a fold-nappe, Betic orogen, southern Spain – Geology 10: 97-102

Platt, J.P. 1983 Progressive refolding in ductile shear zones – J. Struct. Geol. 5: 619-622

Platt, J.P., B. van den Eeckhout, E. Janzen, G. Konert, O.J. Simon & R. Weijermars 1983 The structure and tectonic evolution of the Aguilón fold-nappe, Sierra Alhamilla, Betic Cordilleras, SE Spain – J. Struct. Geol. 5: 519-538

Ramsay, J.G. 1967 Folding and fracturing of rocks – McGraw-Hill (London): 568 pp

Ramsay, J.G. 1980 Shear zone geometry: A review – J. Struct. Geol. 2: 83-99

Ramsay, J.G., M. Casey & R. Kliegfeld 1983 Role of shear in development of the Helvetic fold-thrust of Switzerland – Geology 11: 439-442

Woodcock, N.H. & M.A. Taylor 1983 Randomness testing in three-dimensional orientation data – J. Struct. Geol. 5: 539-548